PRAMANA — journal of physics

Vol. 81, No. 3
September 2013
pp. 511–520

Performance assessment of nanoscale Schottky MOSFET as resonant tunnelling device: Non-equilibrium Green's function formalism

ZAHRA AHANGARI[1,*] and MORTEZA FATHIPOUR[2]

[1]Department of Electrical Engineering, Science and Research Branch, Islamic Azad University, Tehran, Iran
[2]School of Electrical and Computer Engineering, University of Tehran, Tehran, Iran
*Corresponding author. E-mail: z.ahangari@iausr.ac.ir

MS received 2 January 2013; revised 20 April 2013; accepted 11 June 2013

Abstract. A comprehensive study is performed on the electrical characteristics of Schottky barrier MOSFET (SBMOSFET) in nanoscale regime, by employing the non-equilibrium Green's function (NEGF) approach. Quantum confinement results in the enhancement of effective Schottky barrier height (SBH). High enough Schottky barriers at the source/drain and the channel form a double barrier profile along the channel that results in the formation of resonance states. We have, for the first time, proposed a resonant tunnelling device based on SBMOSFET in which multiple resonance states are modulated by the gate voltage. Role of essential factors such as temperature, SBH, bias voltage and structural parameters on the feasibility of this device for silicon-based resonant tunnelling applications are extensively studied. Resonant tunnelling appears at low temperatures and low drain voltages and as a result negative differential resistance (NDR) is apparent in the transfer characteristic. Scaling down the gate length to 6 nm increases the peak-to-valley ratio (PVR) of the drain current. As the effective SBH reduces, the curvature of the double barrier profile is gradually diminished. Therefore, multiple resonant states are contributed to the current and consequently resonant tunnelling is smoothed out.

Keywords. Schottky MOSFET; quantum transport; non-equlibrium Green's function; resonant tunnelling; mode space approach.

PACS Nos 73.30.+y; 73.23.Ad; 85.75.Hh; 85.30.Mn

1. Introduction

Conventional scaled MOSFET with doped source/drain suffers from a high series resistance of ultrashallow source/drain junctions. Schottky barrier source/drain MOSFET (SBMOSFET) is introduced as an alternative to conventional MOSFETs in nanoscale regime [1–5]. As the thickness of the SBMOSFET scales down to a few nanometre,

quantum effects result in the effective SBH enhancement [6–8]. As the effective SBH increases, due to quantum confinement or Fermi level pinning, the source/drain Schottky barriers and the channel form a quantum well in the channel leading to the formation of resonance states in the transport direction [8,9]. Formation of resonance states in the channel has fundamental impact on the current transport in SBMOSFET in nanoscale regime. The main current mechanism in SBMOSFET is tunnelling. Thus, resonant tunnelling is observed through the resonance states in the channel and make SBMOSFET exhibits resonant tunnelling devices. Silicon-based resonant tunnelling devices are used in high-frequency, low-power applications and are compatible with CMOS technology [10,11]. In [8,9] this effect was considered for a fixed SBH = 0.75 eV and resonant tunnelling occurs only for the lowest resonance state due to variation of quantum well curvature by the drain voltage (V_{DS}).

In this paper, we have, for the first time, proposed a resonant tunnelling device based on SBMOSFET in which multiple resonance states are modulated by the gate voltage (V_{GS}), by employing the non-equilibrium Green's function (NEGF) approach. In order to evaluate the feasibility for silicon-based resonant tunnelling devices, it is essential to consider physical and structural requirements which must be accomplished by SBMOSFET. We have extensively discussed important parameters such as temperature, bias voltage, SBH and gate length (L_G) that can affect resonant tunnelling.

The paper is organized as follows: following the introduction in §1, in §2, the numerical simulation approaches are discussed for solving the self-consistent two-dimensional Schrödinger–Poisson equations in the channel. Results and discussions are presented in §3 in which resonant tunnelling phenomena are studied and impact of physical and structural parameters that can influence resonant tunnelling are elucidated as the gate length is gradually reduced to few nanometres. Finally, concluding remarks are presented in §4.

2. Simulation approach

The NEGF formalism and the effective mass approach are employed to simulate quantum transport in nanoscale SBMOSFET. The effective mass of metallic source/drain in the transport direction is chosen the same as that of silicon [6]. Transport is assumed to be ballistic. The structure of the simulated double gate transistor is shown in figure 1a. The thickness of the gate oxide (T_{ox}) and the thickness of the channel (T_{ch}) are 1 nm and 3 nm, respectively. Gate voltage is applied symmetrically to both gates. Transport direction for (1 0 0) wafer is [1 0 0]. The 2D Hamiltonian in the double gate structure is as follows:

$$\left[\frac{-\hbar^2}{2m_x^*}\frac{\partial^2}{\partial x^2} - \frac{\hbar^2}{2m_z^*}\frac{\partial^2}{\partial z^2} + U(x,z)\right]\Psi(x,z) = E(x,z)\Psi(x,z), \tag{1}$$

where m_x^* and m_z^* indicate the effective mass of the electron in the transport direction (x) and the vertical confinement direction (z) respectively. $U(x,z)$ is the 2D electrostatic potential in the channel. There are two approaches for solving this 2D differential equation. In real-space approach which is computationally time consuming, the eigenvalue problem must be solved in all the individual mesh grids in the device [12,13]. Beside real space approach, there is another method called the subband decomposition (mode

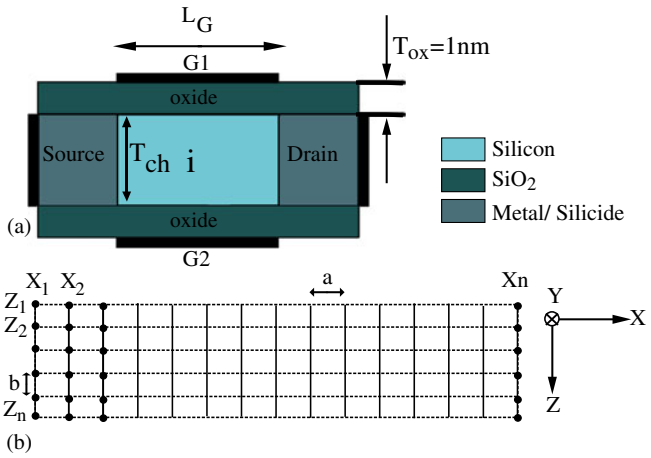

Figure 1. (**a**) Double gate SOI MOSFET with metal source/drain simulated in this study. (**b**) 1D Schrödinger equation is solved in each slice in depth of the channel at each grid in the transport direction.

space) method to solve the 2D Hamiltonian in the channel of SBMOSFET with channel thickness less than 5 nm [13–15].

In mode-space approach 1D Schrödinger equation is solved in each slice along the transverse direction at each grid along the channel (see figure 1b). Hard wall boundary condition is considered in the transverse direction.

$$\left[-\frac{\hbar^2}{2m_z^*}\frac{\partial^2}{\partial z^2}+U(x,z)\right]\psi(x,z)=E_z(x)\psi(x,z). \tag{2}$$

$E_z(x)$ is the eigenenergy or vertical mode and $\psi(x,z)$ is the eigenfunction in the vertical direction at each x grid. Only few modes are considered because modes (subbands) with higher energies are not occupied by the carriers and thus do not contribute to the current. The uncoupled mode-space approach treats electrons in each mode separately because no potential variation in the vertical direction is assumed [13]. For calculating current in the transport direction, Schrödinger equation must be solved with open boundary condition. The energy of the vertical mode is considered as the potential energy along the channel. NEGF formalism is applied to solve the transport problem:

$$\left[\frac{-\hbar^2}{2m_x^*}\frac{\partial^2}{\partial x^2}+E_z(x)\right]\phi_i(x)=E_{\mathrm{L}}(x)\phi_i(x). \tag{3}$$

H_x is defined as

$$H_x=\left[\frac{-\hbar^2}{2m_x^*}\frac{\partial^2}{\partial x^2}+E_z(x)\right]. \tag{4}$$

$E_{\mathrm{L}}(x)$ is the eigenenergy and $\phi_i(x)$ is the eigenfunction along the x direction. The retarded Green's function G for H_x is [16,17]

$$G=\left[E_{\mathrm{L}}(x)I-H_x-\Sigma_{\mathrm{S}}-\Sigma_{\mathrm{D}}\right]^{-1}. \tag{5}$$

Σ is the self-energy which indicates the coupling between the channel and the source/drain reservoirs. Σ_S is the self-energy from the source contact and Σ_D is the self-energy from the drain contact. For calculating electron density, spectral function A is calculated from the retarded Green's function [16]:

$$[A] \equiv i[G - G^{\dagger}] = [A_S] + [A_D], \tag{6}$$

where A_S and A_D are the spectral functions due to the source/drain contacts:

$$A_S = G\Gamma_S G^{\dagger}, \tag{7}$$

$$A_D = G\Gamma_D G^{\dagger}. \tag{8}$$

Γ is the imaginary part of the self-energy and denotes the broadening function. The 2D electron density in the channel for mode (i) at a longitudinal energy E_L is calculated as follows:

$$n_{2Di}(x) = \left(\frac{1}{\hbar a}\right)\sqrt{\frac{2m_y^* k_B T}{\pi}} \int \frac{dE_L}{2\pi} \times \left(A_S F_{-1/2}(E_{FS} - E_L) + A_D F_{-1/2}(E_{FD} - E_L)\right) \tag{9}$$

$$F_{-1/2}(\varepsilon) = \frac{1}{\sqrt{\pi}} \int_0^{\infty} \frac{t^{-1/2} dt}{1 + \exp(t - \varepsilon)}, \tag{10}$$

where F is the Fermi Dirac integral of the order of $-\frac{1}{2}$, T denotes the lattice temperature and $k_B T$ is the Boltzmann constant. E_{FS} and E_{FD} are the source and drain Fermi energies, respectively and a is the grid spacing along x direction and equals to 2 Å.

The potential distribution in the channel is obtained from the Poisson equation. The Poisson equation must be solved self-consistently with the Schrödinger equation. Laplace equation is numerically solved as the initial guess for the potential. This potential is used to calculate the total electron concentration in the channel. Poisson equation uses this electron concentration to update the electrostatic potential building a self-consistent loop until convergence is achieved and a certain error criterion is satisfied. The 2D Poisson equation is as follows:

$$\left(\frac{\partial^2}{\partial x^2} + \frac{\partial^2}{\partial z^2}\right) U(x, z) = -\frac{q^2}{\varepsilon} n_{3D}(x, z), \tag{11}$$

where $n_{3D}(x, z)$ is the total 3D electron concentration in the channel and it is calculated as follows:

$$n_{3Di}(x, z) = \frac{n_{2Di}(x)|\psi_i(x, z)|^2}{b}, \tag{12}$$

where $n_{3Di}(x, z)$ is the 3D electron concentration in real space for mode (i) and it is obtained by multiplying $n_{2Di}(x)$ with the corresponding distribution function $|\psi_i(x, z)|^2/b$. b is the grid spacing along the transverse direction (z) and is equal to 2 Å. The total 3D electron density is obtained by summing $n_{3Di}(x, z)$ over all transverse modes and conduction band valleys that are contributed to the current:

$$n_{3D}(x, z) = \sum_v \sum_i n_{3Di}(x, z). \tag{13}$$

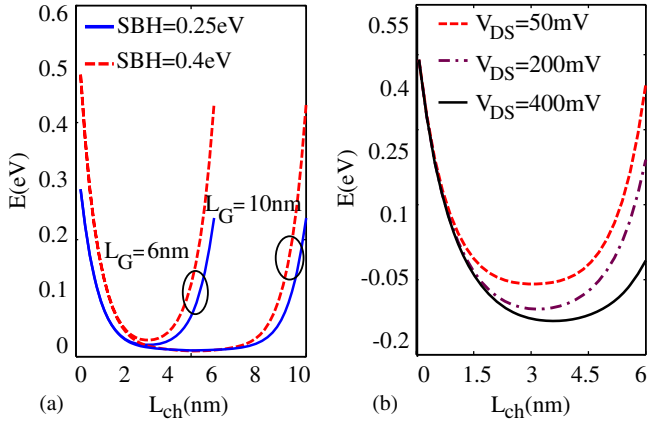

Figure 2. (**a**) Energy of the first subband along the channel for SBH = 0.25 eV and 0.4 eV as the gate length scales down from 10 nm to 6 nm at $V_{DS} = 50$ mV, $V_{GS} = 0.45$ V. (**b**) Impact of drain voltage on the curvature of the lowest subband for SBH = 0.4 eV, $L_G = 6$ nm and $V_{GS} = 0.45$ V. As the drain voltage increases, the curvature of the subband is smoothed out.

For calculating current in SBMOSFET, the transmission probability for energies in the transport direction, $T(E_L)$, with NEGF formalism must be calculated as follows:

$$T(E_L) = \text{trace}(\Gamma_S G\, \Gamma_D G^{\dagger}). \tag{14}$$

The total current for the coherent transport must be summed over all transverse modes and valleys:

$$I_{DS} = \frac{2q}{h} \sum_i \int dE_L T(E_L) \times [F_{-1/2}(E_{FS} - E_L) - F_{-1/2}(E_{FD} - E_L)], \tag{15}$$

$$I_{tot} = \sum_v I_{DS}. \tag{16}$$

3. Results and discussion: Resonant tunnelling effect in SBMOSFET

3.1 *Formation of resonance states along the channel*

As the thickness of SBMOSFET scales down to a few nanometres, quantum effects result in an effective SBH enhancement. The reason is that in ultrathin body fully depleted SOI MOSFET, strong confinement along the transverse direction increases the energy of the first allowed subband. In the case of low drain voltages, high enough SBHs at the source/drain and channel itself form a quantum well. Schottky barriers at the source/drain pull the channel potential towards each other and form a parabolic potential profile along the channel.

Figure 2a compares the first subband profile along the channel for two different SBHs, 0.25 eV and 0.4 eV, at $V_{DS} = 50$ mV and $V_{GS} = 0.45$ V for $T_{si} = 3$ nm as the gate length scales down from 10 nm to 6 nm. As the gate length reduces, the Schottky barriers strongly affect the channel potential and the quantum confinement along the channel is increased. V_D plays an important role in the formation of the quantum well. Figure 2b illustrates the impact of V_{DS} on the profile of the lowest subband along the channel for SBH = 0.4 eV, $L_G = 6$ nm and $V_{GS} = 0.45$ V. For high enough V_{DS}, the curvature of the quantum well is diminished.

Local electron density of states (LDOS) and the lowest subband profile along the channel for SBH = 0.4 eV, $V_{DS} = 50$ mV, $V_{GS} = 0.45$ V when $L_G = 10$ nm and $L_G = 6$ nm is depicted in figures 3a and 3b, respectively. The first subband profile along the channel consists of resonant states. If the subband is constrained in the transport direction, resonant states within the subband will react to this spatial confinement by shifting in energy, depending on the curvature of the subband. The shape of the subband depends on the bias voltages, L_G and the SBH. Energy separation between first and second resonant states increases from 60 meV to 140 meV as L_G scales down from 10 nm to 6 nm. It is worth mentioning that the energy separation between resonant states decreases as the gate voltage increases. Due to discrete resonant states along the channel, resonant tunnelling appears in SBMOSFET due to filling of consecutive resonant states by electrons as the gate voltage is increased. In fact, as long as the energy of electrons in the energy interval between E_{FS} and E_{FD} matches the energy of the localized states in the channel, resonant tunnelling appears.

3.2 *Impact of temperature on resonant tunnelling*

As the temperature increases, the resonance gets smoother due to thermal broadening. Furthermore, it is possible that the current passes through a couple of resonance states

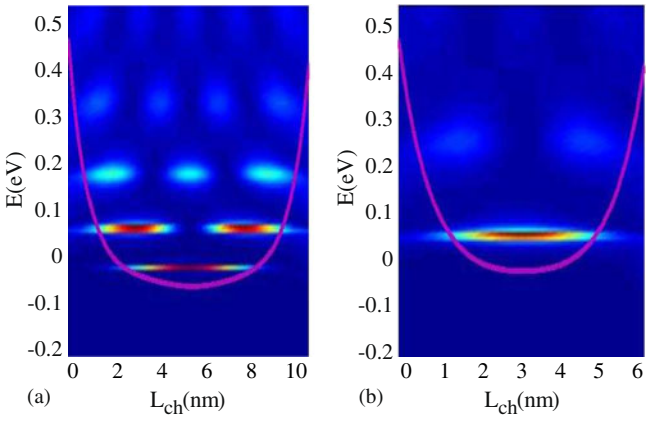

Figure 3. Local electron density of states (LDOS) and first subband profile along the channel at $V_{GS} = 0.45$ V, $V_{DS} = 50$ mV, SBH = 0.4 eV for (**a**) $L_G = 10$ nm and (**b**) $L_G = 6$ nm. As L_G scales down to 6 nm, the energy separation between resonance states increases. Bright regions indicate higher density of states whereas dark blue regions indicate lower density of states.

as the temperature or the drain voltage increases (in this case we have a wider energy range between E_{FS} and E_{FD}), and as a result the resonance is smoothed out. Impact of temperature on the transfer characteristic of nanoscale SBMOSFET with SBH = 0.4 eV, $L_G = 6$ nm and $V_{DS} = 50$ mV is studied (see figure 4a). V_{DS} is chosen as 50 mV in order to help distinguishing current for individual resonant states. Resonant tunnelling appears at low temperatures at $T = 77$ K and 100 K and negative differential resistance region appears in the transfer characteristic. At $T = 400$ K and 77 K, thermal energy is 33 meV and 6.6 meV, respectively. As temperature increases from $T = 77$ K, resonant tunnelling is gradually disappeared due to the thermal energy broadening of carriers and only drain current oscillations are visible in the transfer characteristic. Thermal energy broadening considerably affect DOS and the current. The peak-to-valley ratio (PVR) for the drain current at $T = 77$ K is 1.234 which reduces to 1.18 at $T = 100$ K. Figure 4b presents transconductance (g_m) vs. gate voltage for several temperatures. Transconductance is calculated as the differentiation of drain current with respect to gate voltage at constant drain voltage:

$$g_m = \left.\frac{\partial I_{DS}}{\partial V_G}\right|_{V_D = cte}. \tag{17}$$

Negative g_m implies the occurrence of resonant tunnelling. Owing to adequate high Schottky barriers at the source/drain, a gate-modulated potential well is created along the channel at low drain voltages. Formation of a double barrier profile along the transport direction induces the appearance of resonant states within the potential well. Each time a resonant state is located in the Fermi window, $E_{FS} - E_{FD}$, an increase occurs in the drain current and positive g_m also increases. Gate voltage increment shifts down the resonant states from the Fermi window. Accordingly, an increase in the applied gate voltage

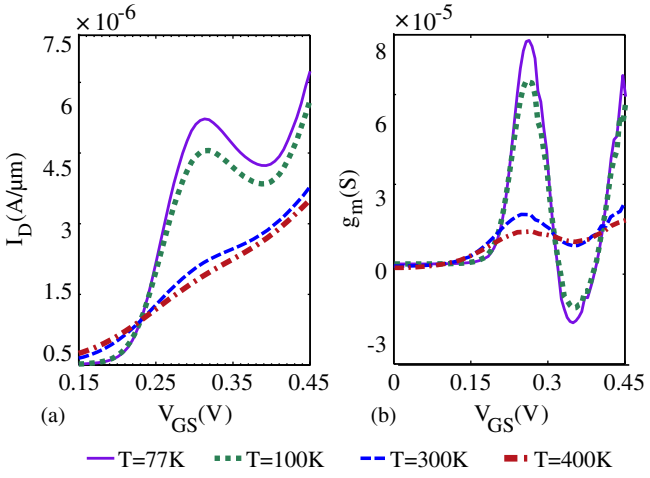

Figure 4. (**a**) I_D–V_{GS} characteristic of SBMOSFET and (**b**) transconductance (g_m) vs. gate voltage for $V_{DS} = 50$ mV, $V_{GS} = 0.45$ V, $L_G = 6$ nm and SBH = 0.4 eV as the temperature varies from 77 K to 400 K. Negative differential resistance is apparent for low temperatures.

produces a proportional decrease in the drain current and there appears 'negative differential resistance' in the transfer characteristic beside an associated negative value of g_m until the consecutive resonant state contributes in current.

At low temperatures, resonant tunnelling and current corresponding to each resonant state are more pronounced. Positive peaks for $T = 300$ K and 400 K in g_m indicate that more resonance states are contributed to the current.

3.3 *Impact of SBH on the curvature of the quantum well channel*

Impact of SBH on resonant tunnelling is studied at $L_G = 6$ nm, $V_{DS} = 50$ mV and $T = 77$ K. As the SBH decreases, resonant tunnelling is gradually disappeared due to the reduction of the quantum well curvature (see figure 5a). Reduction of SBH leads to decrease of energy separation between resonant states. For very low SBHs, the channel will not be similar to a quantum well.

3.4 *Influence of the drain voltage on resonant tunnelling*

Role of drain voltage on the transfer characteristic of SBMOSFET at low temperature ($T = 77$ K) for $L_G = 6$ nm and SBH = 0.4 eV is investigated (see figure 5b).

Resonant tunnelling occurs under certain conditions and changes to direct tunnelling when the curvature of the quantum well channel is diminished or at high temperatures. Resonant tunnelling appears at low drain voltages and low temperatures. For apparent resonant tunnelling in the transfer characteristic, the drain voltage must be smaller than the energy spacing of consecutive resonant states.

At low drain voltages, resonant tunnelling is distinguishable; as V_{DS} increases, several states become involved simultaneously in current and resonant tunnelling is gradually suppressed. Quantum well curvature is smoothed out as V_{DS} increases.

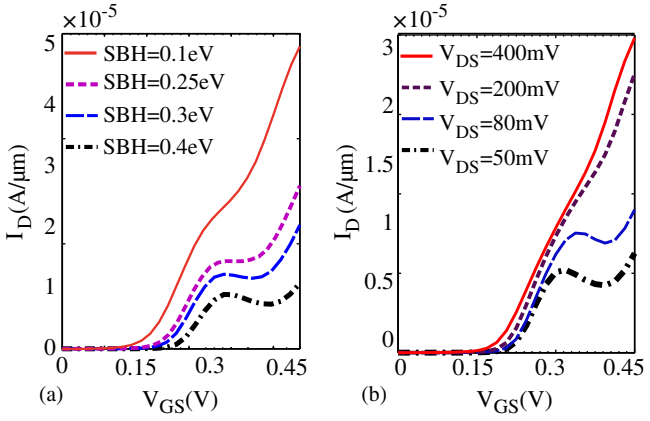

Figure 5. (**a**) Impact of SBH on the transfer characteristic of SBMOSFET for $L_G = 6$ nm, $V_{DS} = 50$ mV and $T = 77$ K. For high effective SBHs resonant tunnelling occurs. (**b**) Impact of drain voltage for SBH = 0.4 eV, $V_{GS} = 0.45$ V and $L_G = 6$ nm. As V_{DS} increases, the curvature of the channel is diminished and resonant tunnelling is gradually suppressed.

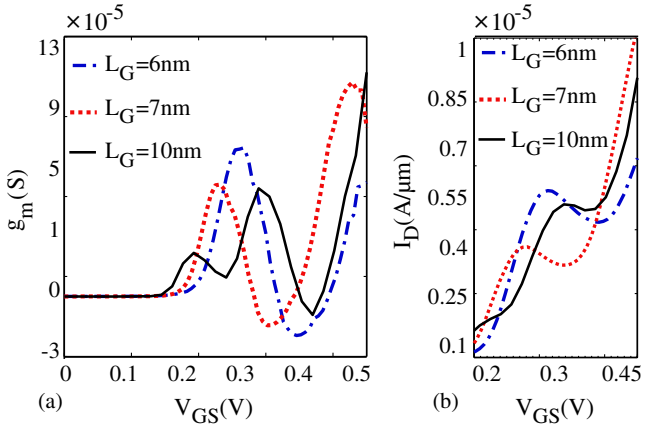

Figure 6. (**a**) Transconductance (g_m) vs. gate voltage and (**b**) $I_{\mathrm{D}}-V_{\mathrm{GS}}$ characteristic of SBMOSFET for $V_{\mathrm{DS}} = 50$ mV, $V_{\mathrm{GS}} = 0.45$ V, SBH $= 0.4$ eV and $T = 77$ K as the channel length scales down from 10 nm to 6 nm. The first resonant tunnelling occurs at higher gate voltages as L_{G} scales down to 6 nm.

3.5 *Role of the gate length*

Figure 6a compares g_m as the gate length scales down from 10 nm to 6 nm for SBH $= 0.4$ eV, $T = 77$ K and $V_{\mathrm{DS}} = 50$ mV. The oscillatory behaviour of g_m reveals the contribution of current to different resonance states. Scaling down the gate length from 10 nm to 6 nm with invariant SBH, increases the peak-to-valley ratio of the current (figure 6b). Gate length has fundamental impact on the profile of quantum well along the channel. The energy spacing of the consecutive resonant states depends upon the gate length. For $L_{\mathrm{G}} = 10$ nm, the energy separation between the resonance states decreases and multiple states with lower energy are contributed to the current (see figure 3a); hence resonant tunnelling is gradually diminished. As the gate voltage increases, resonant tunnelling appears at resonant states with higher energy. When L_{G} scales down from 10 nm to 6 nm, the impact of Schottky barriers on the potential along the channel enhances. Resonant states shift in energy as the confinement in the transport direction enhances and results in higher gate voltages for the occurrence of resonant tunnelling in consecutive resonant states. The maximum PVR for $L_{\mathrm{G}} = 10$ nm at $T = 77$ K is 1.03 which increases to 1.234 for $L_{\mathrm{G}} = 6$ nm.

4. Conclusion

NEGF formalism is employed to study quantum transport in SBMOSFET. We have proposed a novel resonant tunnelling device based on SBMOSFET. As SBMOSFET scales down to nanoscale regime, especially for high effective SBHs, longitudinal quantum confinement appears along the channel and current can only pass through discrete resonant states. Essential parameters that can affect resonant tunnelling in SBMOSFET are investigated. Resonant tunnelling appears at low temperatures and low drain voltages. As

the temperature or the drain voltage increases, multiple resonant states contribute to the current and resonant tunnelling is gradually smoothed out. Scaling down the gate length increases the energy of consecutive resonant states resulting in higher peak-to-valley ratio (PVR) of the drain current. We have extensively clarified the feasibility of silicon-based ultrascaled SBMOSFET as a resonant tunnelling device that is compatible with existing technology.

References

[1] R S Xiong, T J King and J Bokor, *IEEE Trans. Electron Devices* **52(8)**, 1859 (2005)
[2] R A Vega, *IEEE Trans. Electron Devices* **53(4)**, 866 (2006)
[3] S Zhu, J Chen, M F Li, S J Lee, J Singh, C X Zhu, A Du, C H Tung, A Chin and D L Kwong, *IEEE Elec. Dev. Lett.* **25(8)**, 565 (2004)
[4] J M Larson and J P Synder, *IEEE Trans. Electron Devices* **53**, 1048 (2006)
[5] Y Nishi, A Kinoshita, D Hagishima and J Koga, *Jpn. J. Appl. Phys.* **47(1)**, 99 (2008)
[6] J Guo and M Lundstrom, *IEEE Trans. Electron Devices* **49(11)**, 1897 (2002)
[7] A Afzalian and D Flandre, *Solid-State Electron.* **65**, 123 (2011)
[8] S Toriyama, *Jpn. J. Appl. Phys.* **49**, 104204 (2010)
[9] S Toriyama and N Sano, *J. Comput. Electron.* **7**, 471 (2008)
[10] E Buccafurri, A Medjahdi, F Calmon, R Clerc, M Pala, A Poncet and G Ghibaudo, *Proc. ESSCIRC* (2009), pp. 220–223
[11] E Buccafurri, R Clerc, F Calmon, M Pala, A Poncet and G Ghibaudo, *Proc. Int. Conference on Ultimate Integration of Silicon (ULIS)* (2009), pp. 91–94
[12] Z Ren, R Venugopal, S Goasguen and S Datta, *IEEE Trans. Electron Devices* **50(9)**, 1914 (2003)
[13] R Venugopal, Z Ren, S Datta, M S Lundstrom and D Jovanovic, *J. Appl. Phys.* **92(7)**, 3730 (2002)
[14] A Afzalian, N Dehdashti Akhavan, C W Lee, R Yan, I Ferain, P Razavi and J P Colinge, *J. Comput. Electron.* **8**, 287 (2009)
[15] Y M Sabry, T M Abdolkader and W F Farouk, *Proc. Int. Conference on Microelectronics (ICM)* (2007)
[16] S Datta, *Quantum transport: Atom to transistor* (Cambridge University Press, Cambridge, 2005)
[17] S Datta, *Superlattices and Microstructures* **28(4)**, 253 (2003)